CHIN. PHYS. LETT. Vol. 37, No. 9 (2020) 097301

Model Hamiltonian for the Quantum Anomalous Hall State in Iron-Halogenide

Qian Sui(眭茜)[1†], Jiaxin Zhang(张嘉鑫)[1,2†], Suhua Jin(金粟华)[1†], Yunyouyou Xia(夏云悠悠)[1], and Gang Li(李刚)[1,3*]

[1]*School of Physical Science and Technology, ShanghaiTech University, Shanghai 200031, China*
[2]*Institute for Advanced Study, Tsinghua University, Beijing 100084, China*
[3]*ShanghaiTech Laboratory for Topological Physics, ShanghaiTech University, Shanghai 200031, China*

(Received 14 June 2020; accepted 16 July 2020; published online 1 September 2020)

We examine quantum anomalous Hall (QAH) insulators with intrinsic magnetism displaying quantized Hall conductance at zero magnetic fields. The spin-momentum locking of the topological edge stats promises QAH insulators with great potential in device applications in the field of spintronics. Here, we generalize Haldane's model on the honeycomb lattice to a more realistic two-orbital case without the artificial real-space complex hopping. Instead, we introduce an intraorbital coupling, stemming directly from the local spin-orbit coupling (SOC). Our $d_{xy}/d_{x^2-y^2}$ model may be viewed as a generalization of the bismuthene p_x/p_y-model for correlated d-orbitals. It promises a large SOC gap, featuring a high operating temperature. This two-orbital model nicely explains the low-energy excitation and the topology of two-dimensional ferromagnetic iron-halogenides. Furthermore, we find that electronic correlations can drive the QAH states to a $c = 0$ phase, in which every band carries a nonzero Chern number. Our work not only provides a realistic QAH model, but also generalizes the nontrivial band topology to correlated orbitals, which demonstrates an exciting topological phase transition driven by Coulomb repulsions. Both the model and the material candidates provide excellent platforms for future study of the interplay between electronic correlations and nontrivial band topology.

PACS: 73.43.−f, 03.65.Vf, 73.20.−r, 73.22.−f DOI: 10.1088/0256-307X/37/9/097301

The discovery of the mystery integer steps in the conductance of quantum Hall insulators[1] opens the door to a previously unexplored topological realm.[2,3] Each state differs from another by virtue of its topological property rather than in terms of symmetry. For the quantum Hall insulator, the topological character is known as the Chern or TKNN number,[4] which fundamentally relates to the Berry curvature of all occupied bands.[5] Haldane's model[6] was the first model to realize quantum Hall states without Landau levels, i.e., the so-called quantum anomalous Hall (QAH) insulators. In addition to nearest-neighbor hopping, Haldane introduced second nearest-neighbor hopping terms with opposite phases on AB sublattices so as to break the time-reversal symmetry. Although Haldane stated in his paper that this particular model is unlikely to be directly physically realizable, it correctly associates the mystery QHE with the broken time-reversal symmetry, providing a gateway to an unexpectedly rich area of topological physics.[7−12] In Haldane's model, different topological phases are monitored by the Berry curvatures at the two independent Brillouin zone (BZ) corner $\boldsymbol{K}$ and $\boldsymbol{K}'$. The transition between states with different topologies is controlled by the different signs of the curvature rather than by symmetry, i.e., in QAH states the Berry curvatures at $\boldsymbol{K}$ and $\boldsymbol{K}'$ are of the same sign, while they are opposite in the trivial insulating phase. Pioneered by Haldane's work, quantum spin Hall (QSH) states were soon proposed as a superposition of two QAH insulators with equal but opposite magnetic moments.[13] As a consequence, the time-reversal symmetry is restored, and the Berry curvature remains nonzero at one of the time-reversal paired states. The complex hopping is replaced by the SOC, which significantly extends the topological concept of Haldane's model to realistic material systems. Experimentally, HgTe/CdTe quantum well[14,15] was the first discovered QSH insulator whose topology is controlled by the thickness of HgTe and, microscopically, by the inversion of the Γ_6 and Γ_8 states. In addition to the band-inversion mechanism, a graphene-type QSH insulator, possessing a large gap,[16−18] and with local spin-orbital coupling (SOC) has also recently been discovered, which even features spintronic applications at room temperature.

Compared to the discovery of intrinsic QSH insulators, QAH states are much more challenging to achieve experimentally, as the process usually requires extremely low temperature and a high degree of experimental skill.[19−21] One feasible experimental approach is to dope the topological insulators with dilute magnetic impurities. Long-range ferromagnetic order can be established via a surface RKKY-type interaction,[22] the Bloembergen–Rowland,[23,24] or the van Vleck mechanism.[25] These delicate experimental procedures impose strong constraints, such

Supported by the National Key R&D Program of China (Grant No. 2017YFE0131300), the Strategic Priority Research Program of Chinese Academy of Sciences (Grant No. XDA18010000), the Starting Grant of ShanghaiTech University, and the Program for Professor of Special Appointment (Shanghai Eastern Scholar).
†These three authors contributed equally to this work.
*Corresponding author. Email: ligang@shanghaitech.edu.cn
© 2020 Chinese Physical Society and IOP Publishing Ltd

that they can only be accomplished by a small number of groups. Furthermore, breaking time-reversal symmetry ($\mathcal{T}$) in this way does not decouple the conceptual two copies of QAH states, but rather inverts one copy back to the normal band order while keeping the other one inverted. Recently, quantized Hall conductance was experimentally observed in van der Waals (vdW) stacked antiferromagnetic (AFM) $MnBi_2Te_4$.[26–32] The intrinsic magnetism and the vdW-type structure of $MnBi_2Te_4$ may fundamentally reveal a brand new, yet experimentally controllable routine by inserting magnetic layers into topological insulators, which would substantially lower the barrier to the experimental realization of QAH, and possesses a more promising application potential.

In this Letter, we provide a more realistic QAH lattice model by extending Haldane's model to two-orbital systems with finite local SOC. We thereby demonstrate three distinct topological phases, where $c = 0$, $c = -1$, and $c = 2$. This model elegantly explains a class of two-dimensional ferromagnetic materials which are large-gap QAH material candidates exhibiting strong potential for room-temperature applications. Furthermore, a topological phase transition occurs with an increase in electronic interactions. The $c = -1$ phase transforms to the $c = 0$ phase with a nonzero band Chern number.

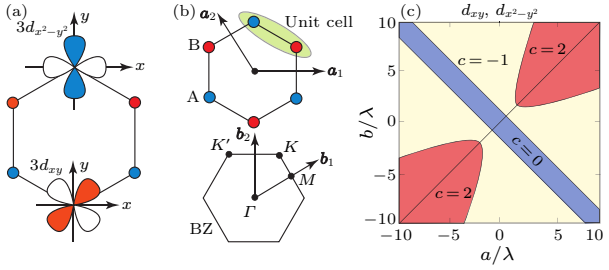

Fig. 1. Illustration of a two-orbital model on a Honeycomb lattice, and the corresponding phase diagram: (a) $d_{xy} - d_{x^2-y^2}$ model, (b) the Honeycomb lattice and the corresponding BZ. The lattice and reciprocal vectors are defined as $\boldsymbol{a}_1 = (1, 0)$, $\boldsymbol{a}_2 = (-\frac{1}{2}, \frac{\sqrt{3}}{2})$, $\boldsymbol{b}_1 = (2\pi, \frac{2\sqrt{3}\pi}{3})$, $\boldsymbol{b}_2 = (0, \frac{4\sqrt{3}\pi}{3})$. (c) The phase diagram of the proposed model as functions of the parameters a/λ and b/λ.

Results. Following Haldane's model, we consider a tight-binding model for fully spin-polarized electrons on a honeycomb lattice, as shown in Fig. 1(a). Here, only nearest neighbor hopping is considered. Clearly if only one orbital exists, one can obtain a trivial model, with the linear band crossing at the $\boldsymbol{K}$ and $\boldsymbol{K}'$ points, which is the model for graphene. Haldane introduced a system of complex hopping, connecting AA and BB sublattices, on which electrons travel in opposite directions. Depending on the phase of the complex hopping, topological phase transitions can occur between trivial states and nontrivial QAH states. We aim at a realistic construction of a QAH model with the potential to be realized in material systems. For this reason, we consider d_{xy} and $d_{x^2-y^2}$ orbitals. The reason for this particular choice of orbital combination is explained below. Here, we use $t^{\mathrm{AB}}_{\alpha\beta}$ to represent the hopping amplitude between orbitals α/β, i.e., $d_{xy}/d_{x^2-y^2}$, at the two inequivalent sites A/B. The general two-orbital tight-binding Hamiltonian on a honeycomb lattice takes the following form:

$$H_0 = \left(\begin{array}{cc|cc} \epsilon^{\mathrm{A}}_{\alpha} & 0 & h^{\mathrm{AB}}_{\alpha\alpha} & h^{\mathrm{AB}}_{\alpha\beta} \\ 0 & \epsilon^{\mathrm{A}}_{\beta} & h^{\mathrm{AB}}_{\beta\alpha} & h^{\mathrm{AB}}_{\beta\beta} \\ \hline h^{\mathrm{BA}}_{\alpha\alpha} & h^{\mathrm{BA}}_{\alpha\beta} & \epsilon^{\mathrm{B}}_{\alpha} & 0 \\ h^{\mathrm{BA}}_{\beta\alpha} & h^{\mathrm{BA}}_{\beta\beta} & 0 & \epsilon^{\mathrm{B}}_{\beta} \end{array}\right), \tag{1}$$

where the diagonal matrix element $\epsilon^{A/B}_{\alpha/\beta} = \epsilon$ represents the orbital potential of α/β at site A/B. These are taken to be equal in our calculations, which control the position of the linear band crossing at $\boldsymbol{K}$ and $\boldsymbol{K}'$ when there is no SOC. Off-diagonal $h^{\mathrm{AB}}_{\alpha\beta}$ denotes the Hamiltonian element formed by hopping $t^{\mathrm{AB}}_{\alpha\beta}$. One simple way to correctly account for the orbital symmetry is to follow the Slater–Koster table,[33] from which one can easily obtain $h^{\mathrm{AB}}_{\alpha\alpha} = M_1(1 + e^{ik_1}) + M_2 e^{-ik_2}$, $h^{\mathrm{AB}}_{\beta\beta} = M_3(1+e^{ik_1})+M_4 e^{-ik_2}$, $h^{\mathrm{AB}}_{\alpha\beta} = \sqrt{3}M_5(1-e^{ik_1})$. Here, k_1 and k_2 are the fractions of reciprocal lattice vectors $\boldsymbol{b}_1$ and $\boldsymbol{b}_2$. The Hamiltonian is Hermitian, as $h^{\mathrm{BA}}_{\alpha\beta} = (h^{\mathrm{AB}}_{\alpha\beta})^*$ and $h^{\mathrm{AB}}_{\beta\alpha} = h^{\mathrm{AB}}_{\alpha\beta}$. The corresponding coefficients $(M_1 \cdots M_5)$ are not independent, and are parameterized via the standard Slater–Koster integrals as $M_1 = (3a+b)/4$, $M_2 = b$, $M_3 = (a+3b)/4$, $M_4 = a$ and $M_5 = (a-b)/4$, where $a = (3V^1_{dd\sigma} + V^1_{dd\delta})/4$ and $b = V^1_{dd\pi}$.

The proposed orbital combination is of particular importance in relation to the topological nature of the system, as it allows non-vanishing local SOC term, which is usually the largest SOC contribution available, which is the reason for selecting this specific orbital combination. Given the atomic SOC $\lambda \boldsymbol{L} \cdot \boldsymbol{S}$, we find a constant expectation value between the different orbital states, proportional to strength λ, with zero contribution between the same orbitals. This can easily be seen given the expression of d_{xy} and $d_{x^2-y^2}$ in terms of complex spherical harmonics $Y_2^{\pm 2}$ and $\boldsymbol{L}\cdot\boldsymbol{S}$ as the ladder operators:

$$d_{xy,\sigma} = i\sqrt{\frac{1}{2}}\,(Y_2^{-2} - Y_2^2)_\sigma, \tag{2}$$

$$d_{x^2-y^2,\sigma} = \sqrt{\frac{1}{2}}\,(Y_2^{-2} + Y_2^2)_\sigma, \tag{3}$$

$$\boldsymbol{L}\cdot\boldsymbol{S} = \frac{L^+S^- + L^-S^+}{2} + L_zS_z. \tag{4}$$

Here, σ denotes the spin, with ± 1 for up/down states. As $L^\pm$ only connect two states which differ by $m = \pm 1$, their matrix elements vanish between any combination of the two orbitals $d_{xy,\sigma}$ and $d_{x^2-y^2,\sigma}$. In contrast, L_zS_z preserves spin and has a nonzero matrix element between the two states:

$$\begin{aligned} &{}_\sigma\langle d_{xy}|L_zS_z|d_{xy}\rangle_\sigma \\ &= \frac{1}{2}[Y_2^{-2} - Y_2^2]\cdot[-2Y_2^{-2} - 2Y_2^2]\cdot\sigma = 0, \end{aligned} \tag{5a}$$

$$_{\sigma}\langle d_{xy}|L_zS_z|d_{x^2-y^2}\rangle_{\sigma}$$
$$= -\frac{i}{2}[Y_2^{-2} - Y_2^2]\cdot[-2Y_2^{-2} + 2Y_2^2]\cdot\sigma = 2i\sigma. \quad (5b)$$

In this work, we consider the fully polarized spin-↑ component; the leading SOC term between d_{xy} and $d_{x^2-y^2}$ orbitals are, therefore expressed as follows:

$$\langle d_{xy}|\lambda \boldsymbol{L}\cdot\boldsymbol{S}|d_{x^2-y^2}\rangle = 2i\lambda. \quad (6)$$

This resembles the p_x/p_y model of bismuthene,[16–18] where the large topological gap derived from the local SOC makes it a good material candidate for room-temperature spintronic applications. By breaking inversion symmetry, one can further introduce Rashba-type SOC to the model, as carried out in the bismuthene p_x/p_y model. In this work, we concentrate on the Hamiltonian $H_{\rm qah}(k) = H_0(k) + \lambda \boldsymbol{L}\cdot\boldsymbol{S}$ for the sake of simplicity, and neglect other types of SOC which do not affect the topological nature of the models.

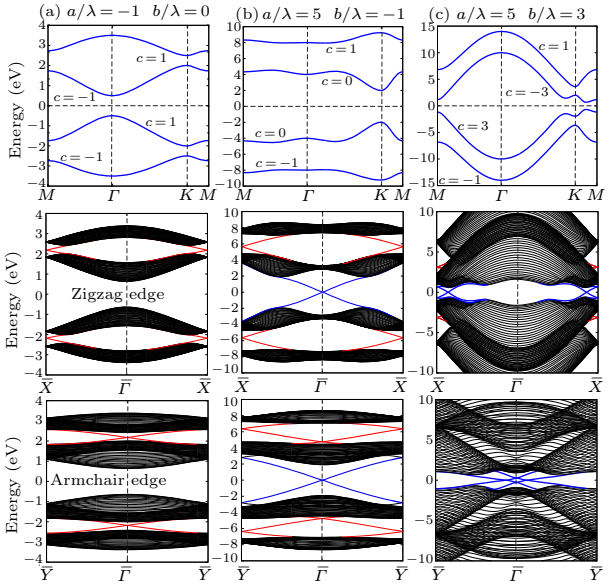

Fig. 2. The bulk and edge electronic structures of the $d_{xy}/d_{x^2-y^2}$ model in three topologically different phases: (a) $c=0$, (b) $c=-1$, (c) $c=2$.

Equations (1) and (6) constitute our QAH Hamiltonian, whose generic phase diagram as functions of a and b is shown in Fig. 1(c). Chern number calculations indicate a rich topological phase diagram of this fully polarized tight-binding model. Except for the small regime around $a=-b$ and $a=b$, large areas in the parameter spaces host topologically nontrivial states, and two distinct phases are discovered, with $c=-1$ and $c=2$. In Fig. 2 we further display examples of all three topologically distinct phases with distinctive band and edge electronic structures. We explicitly determine the Chern number for each band. The phase diagram shown in Fig. 1(c) is obtained from the sum of the Chern numbers of the two occupied bands. From the bulk-boundary correspondence, the Chern number indicates precisely the number of edge modes. Interestingly, even for the $c=0$ phase in Fig. 1(c), the topology of each band is nontrivial. As shown in Fig. 2(a), despite the zero net Chern number of the two occupied bands, each band carries a nonzero topological invariant, allowing the presence of a nontrivial edge mode. Thus, the gap between the first and second bands, as well as the gap between the third and fourth bands, host topological edge states. From $c=0$ to $c=-1$ phases, the gap between the second and the third band closes and reopens at the Γ point. From $c=-1$ to $c=2$ phases, a similar closing and reopening of the gap occurs at the M point. Both Γ and M are time-reversal invariant momenta of the honeycomb lattice. Consequently, the topology of the model changes when the gap closes and reopens at these points. Note that, for the $c=2$ phase, along each edge, there are two edge modes; these connect the valence with conduction bands around the M point, rather than Γ along the zigzag edge.

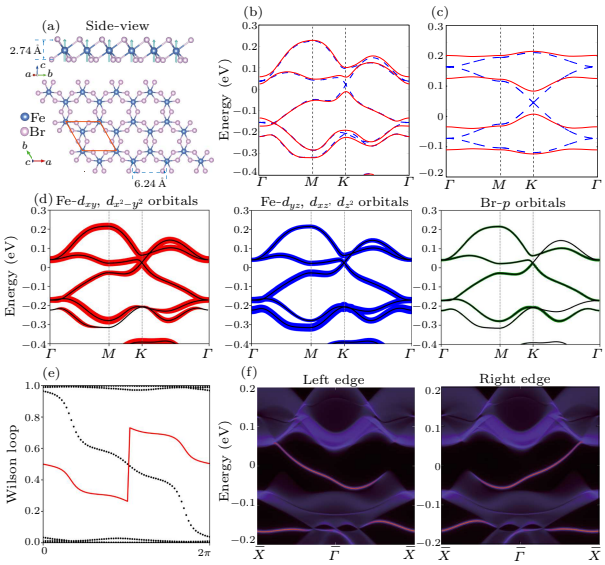

Fig. 3. (a) Structural model of monolayer $FeBr_3$ in side and top views. The iron atoms form an effective honeycomb lattice. (b) Electronic structure with (red solid line) and without (blue dashed line) SOC. (c) The model bands with fitting parameters from Table 1. (d) The projection of Bloch bands on the atomic-like orbitals indicates that around K/K', $d_{xy}/d_{x^2-y^2}$ orbitals dominate. (e) The Wilson loop shows $c=-1$. (f) Calculations of edge states for left and right edges, which are both terminated with zigzag geometry.

Table 1. Model parameters for different two-dimensional ferromagnetic semiconductors hosting a large-gap QAH phase. Here a, b, λ, ϵ are the model parameters defined in equations (1) and (6) in units of meV. Δ is the size of the topological gap.

	$FeCl_3$	$FeBr_3$	FeI_3	$Fe_2Br_3I_3$	$Fe_2Cl_3I_3$	$Fe_2Cl_3Br_3$
a	94.1	85.2	82	88	105	96.6
b	−28.9	−14.2	−5.8	−7.9	−16.5	−36.8
λ	17.5	17.2	10.3	14	17.3	17.3
Δ	70	68	41	56	69	69
ϵ	16	20	27	34	24	17

Material Candidates. The proposed correlated QAH model neatly explains a class of two-dimensional ferromagnetic semiconductors, represented by $FeBr_3$, which was recently proposed as a large-gap QAH

insulator.[34] However, we wish to emphasize that this is not the only material candidate which realizes the topological physics of the proposed tight-binding model. On a honeycomb lattice, as long as the low energy physics around K/K' is determined by $d_{x^2-y^2}/d_{xy}$ orbitals, the proposed model can be applied. With its guidance, we can manually replace Br with other elements in group-VII without affecting the low-energy d-orbitals of iron. Consequently, we find a class of large-gap QAH candidate materials including $FeCl_3$, FeI_3, $Fe_2Cl_3Br_3$, $Fe_2Cl_3I_3$, and $Fe_2Br_3I_3$, all of which resemble the $c = -1$ QAH phase of our model. By fitting our model to the density functional theory calculations, and further requiring them to coincide at the Γ and K points, we obtain the model parameters listed in Table 1.

The first-principles calculations in this work were carried out by employing the Vienna *ab initio* simulation package (VASP), using the projector augmented wave (PAW) method.[35] The generalized gradient approximation (GGA), as implemented in the Perdew–Burke–Ernzerhof (PBE) functional[36] was adopted in both structure relaxation and band structure calculations. The cutoff parameter for the wave functions was set to be 400 eV. The Brillouin zone (BZ) was sampled by the gamma-centered method with a k-mesh $7 \times 7 \times 1$. To obtain the stable structure, we allow both the atomic positions and the in-plane lattice constant to relax while keeping the total volume of the system unchanged. The energy and force convergence criteria were set to 10^{-7} eV and -10^{-3} eV/Å, respectively. The initial lattice constant, atomic positions, and layer distance were taken from the corresponding bulk structures. The surface states and the Wilson loop were calculated using our in-house code TMC (Topological Material Calculation library) with the iterative Green's function approach[37] based on the maximally localized Wannier functions[38] obtained through the VASP2WANNIER90.[39]

In Fig. 3 we take $FeBr_3$ as an example. The local 3-fold rotation symmetry and the mirror symmetry are maintained, which is essential for reserving the linear band crossing at $\boldsymbol{K}$ and $\boldsymbol{K'}$ on a honeycomb lattice without SOC. Subsequently, the SOC opens a gap of 36 meV, as shown in Fig. 3(b), which is sufficiently large for room-temperature experiments and applications. The corresponding model electronic structure with/without SOC is shown in Fig. 3(c), which effectively captures the essential topology of the two occupied and two unoccupied states. The calculated Chern number is -1 for the two occupied bands. Individually, the four bands carry $c = -1$, $c = 0$, $c = 0$ and $c = 1$, respectively. We further terminated the system with a zigzag edge, determining the edge states correspondingly, as shown in Figs. 3(f)–3(g). As anticipated, compared to the bulk bands, both edges develop topologically nontrivial modes, confirming this system as a QAH insulator. It should be further noted that, in addition to the topological edge states around the Fermi level, a further QAH edge mode also exists between the first and second valence bands. This exactly resembles the $c = -1$ phase of our model Hamiltonian [see Fig. 2(b) for the bulk and edge electronic structures].

In addition to $FeBr_3$, other systems, including $FeCl_3$, FeI_3, $Fe_2Cl_3Br_3$, $Fe_2Cl_3I_3$, and $Fe_2Br_3I_3$ all display similar electronic structures and topological natures. The hypothetical engineering of halogenide atoms would not affect the low-energy excitation of these monolayer systems. Thus, the proposed QAH model applies equally to them. The relaxed crystal structures, bulk electronic structures, and the corresponding edge states along a zigzag termination are shown in Fig. 4. The corresponding model parameters can be found in Table 1.

Electronic Correlations and Topological Phase Transition. As discussed above, our two-orbital model neatly explains the low-energy excitations and the topology of two-dimensional iron-halogenides. In addition to promoting long-range ferromagnetism, the localized d-orbitals also favor electron–electron interactions. To understand the interplay of electronic correlation with nontrivial band topology in an *ab initio* way, we further performed DFT+U calculations via Dudarev's approach. We found that the spin-polarized low-spin ground state without SOC is stable up to $U \sim 6$ eV. Above 6 eV, the high-spin states always win, and the electronic structure becomes completely different, which falls outside the scope of this discussion. In Fig. 5, we show the results for three different values of U. For all other values of U, qualitatively similar band structures are obtained. Notably, the linear band crossing at K/K' is unaffected by U. However, the joint operation of SOC and electronic correlations in iron halogenides will strongly modify their electronic structures. The topological character is quickly lost around 0.5 eV, i.e., there is no edge state around the Fermi level. The system transforms into a new phase, in which the total Chern number of all bands below the Fermi level is zero. However, we need to emphasize that this system is not trivial at all. Actually, every band carries a nonzero band Chern number. It is only because the their sum is zero up to the Fermi level that we lose the topological edge states for U greater than $\sim$0.5 eV. Due to the nonzero Chern number of each band, topological states exist within other gaps. For example, one can observe topological edge states between the first and the second valence bands, as well as between the first and second conduction bands. Their presence confirms the nontrivial topology of the system. By tuning the chemical potential into these gaps, the system transforms back to a topological phase. Figure 5 shows an interaction-driven topological phase transition from a $c = -1$ to a $c = 0$ phase, where the final states carry completely different band Chern numbers. The competition and interplay of electronic correlations with nontrivial band topology is an important but less-explored topic, partly due to the lack of appropriate models and material playgrounds. In this sense, our work provides an excellent platform for both theoretical and experimental studies of electronic correlation and topology.

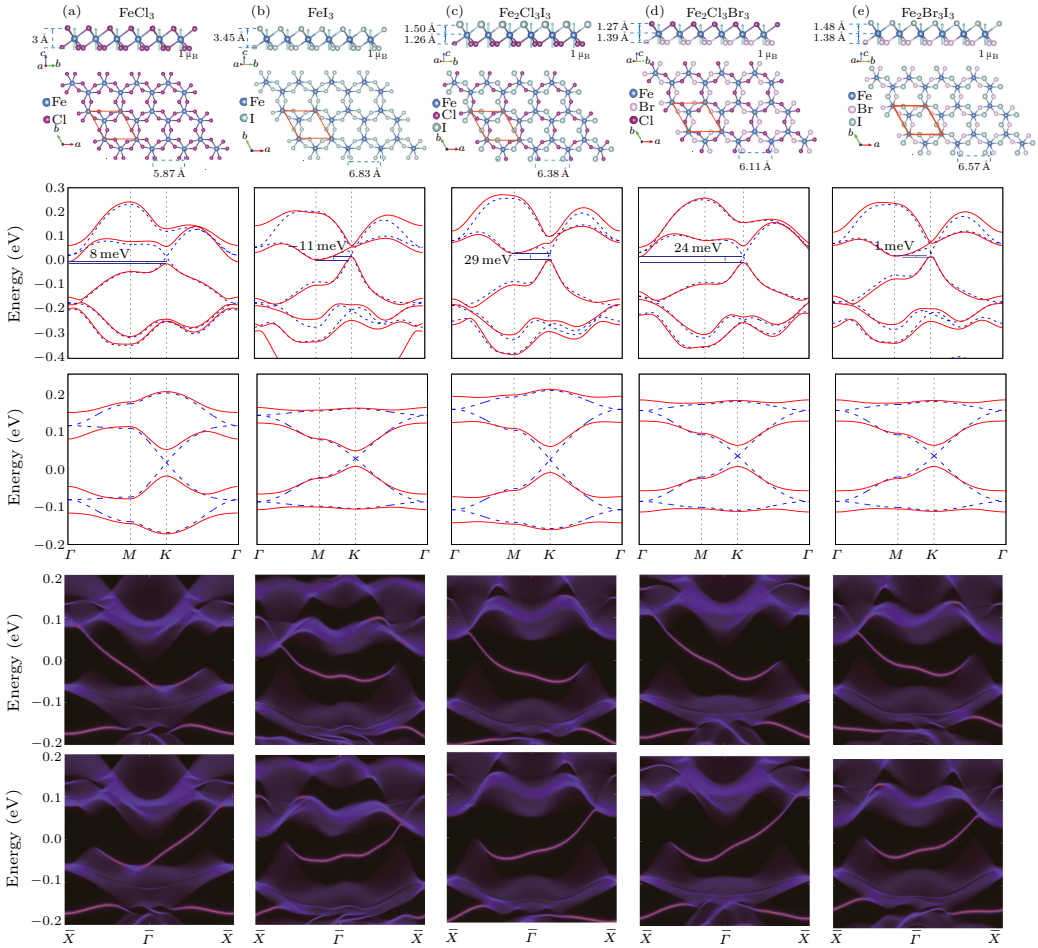

Fig. 4. Crystalline and monolayer electronic structures and corresponding edge states of $FeCl_3$, $Fe_2Cl_3I_3$, FeI_3, $Fe_2Cl_3Br_3$ and $Fe_2Br_3I_3$. The five rows for each material represent the relaxed crystal structure, the bulk electronic structure from first-principles calculations, the eigenvalues of the fitted model, and the left/right edge states, corresponding to a zigzag termination.

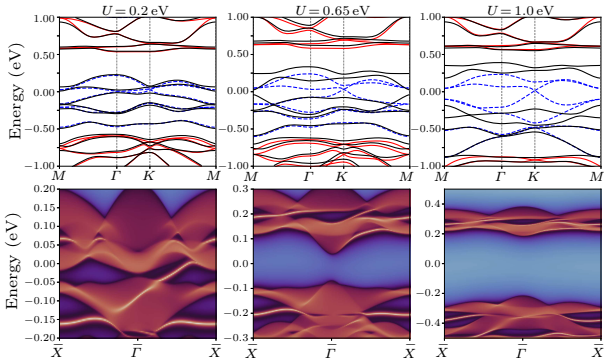

Fig. 5. Electron structures of $FeBr_3$, calculated via DFT+U with three different U values. The red solid and blue dashed lines respectively denote the band structures in the absence of SOC. The black solid line corresponds to the bands calculated with SOC. The second row shows the corresponding edge states, from which a topological phase transition can be identified between $U = 0.2$ eV and 0.65 eV.

Discussions. We have demonstrated the validity of the new QAH model in relation to monolayer iron-halogenides, due to their correlated d-orbitals and the promise of a large topological gap. Experimentally, $FeBr_3$, $FeCl_3$, and FeI_3 crystallize in van der Waals quasi two-dimensional form, and their successful syntheses have previously been reported.[40–43] Due to their weak interlayer coupling, it is highly feasible to cleave these materials to realize the promising QAH states discussed above. The thermal and dynamical stabilities of their monolayers have also been confirmed theoretically by different groups.[44,45] We note that their bulk materials have completely different electronic structures as compared to the monolayers, indicating a three-dimensional nature. We also note that the change in their electronic structure stems from changes to the magnetic configuration of these systems. A low-to-high spin phase transition occurs in these systems with an increase in sample thickness. The ground states of the thin film and the bulk are in low-spin and high-spin states of iron d-electrons. The increase of film thickness reduces the energy gap between t_{2g} and e_g states, with the latter lying below. Thus, a low-spin configuration of iron d^5 with $S_{\text{eff}} = 1/2$ at the thin-film limit will change to a high-spin arrangement, where $S_{\text{eff}} = 5/2$, in the bulk materials. This alteration in electronic structure is not due to a strong interlayer coupling. Thus, we believe that the mechanical cleavage is straightforward.

In summary, we have proposed a generic tight-binding model, consisting of two correlated orbitals

$d_{xy}/d_{x^2-y^2}$, possessing a large local SOC strength. This model displays a rich phase diagram with three distinct topological states. One of these topological phases is shown to be realized in a class of two-dimensional ferromagnetic insulators, which display a large-gap QAH state with potential for possible room-temperature spintronic applications. On the application of interaction, these systems also show a novel topological phase transition, driven by electronic correlations. The coexistence of correlated d-orbitals and QAH states make this model an ideal system with which to study the correlation effect on topological insulators.

Calculations were carried out at the HPC Platform of ShanghaiTech University Library and Information Services, and at the School of Physical Science and Technology.

References

[1] Klitzing K V, Dorda G and Pepper M 1980 *Phys. Rev. Lett.* **45** 494
[2] Hasan M Z and Kane C L 2010 *Rev. Mod. Phys.* **82** 3045
[3] Qi X L and Zhang S C 2011 *Rev. Mod. Phys.* **83** 1057
[4] Thouless D J, Kohmoto M, Nightingale M P and den Nijs M 1982 *Phys. Rev. Lett.* **49** 405
[5] Berry M V 1984 *Proc. R. Soc. London A* **392** 45
[6] Haldane F D M 1988 *Phys. Rev. Lett.* **61** 2015
[7] Po H C, Vishwanath A and Watanabe H 2017 *Nat. Commun.* **8** 50
[8] Watanabe H, Po H C and Vishwanath A 2018 *Sci. Adv.* **4** eaat8685
[9] Bradlyn B, Elcoro L, Cano J, Vergniory M G, Wang Z, Felser C, Aroyo M I and Bernevig B A 2017 *Nature* **547** 298
[10] Tang F, Po H C, Vishwanath A and Wan X 2019 *Nature* **566** 486
[11] Zhang T, Jiang Y, Song Z, Huang H, He Y, Fang Z, Weng H and Fang C 2019 *Nature* **566** 475
[12] Vergniory M G, Elcoro L, Felser C, Regnault N, Bernevig B A and Wang Z 2019 *Nature* **566** 480
[13] Kane C L and Mele E J 2005 *Phys. Rev. Lett.* **95** 146802
[14] Bernevig B A, Hughes T L and Zhang S C 2006 *Science* **314** 1757
[15] König M, Wiedmann S, Brüne C, Roth A, Buhmann H, Molenkamp L W, Qi X L and Zhang S C 2007 *Science* **318** 766
[16] Reis F, Li G, Dudy L, Bauernfeind M, Glass S, Hanke W, Thomale R, Schäfer J and Claessen R 2017 *Science* **357** 287
[17] Li G, Hanke W, Hankiewicz E M, Reis F, Schäfer J, Claessen R, Wu C and Thomale R 2018 *Phys. Rev. B* **98** 165146
[18] Dominguez F, Scharf B, Li G, Schäfer J, Claessen R, Hanke W, Thomale R and Hankiewicz E M 2018 *Phys. Rev. B* **98** 161407
[19] Chang C Z, Zhang J, Feng X, Shen J, Zhang Z, Guo M, Li K, Ou Y, Wei P, Wang L L, Ji Z Q, Feng Y, Ji S, Chen X, Jia J, Dai X, Fang Z, Zhang S C, He K, Wang Y, Lu L, Ma X C and Xue Q K 2013 *Science* **340** 167
[20] Jiang G, Feng Y, Wu W, Li S, Bai Y, Li Y, Zhang Q, Gu L, Feng X, Zhang D, Song C, Wang L, Li W, Ma X C, Xue Q K, Wang Y and He K 2018 *Chin. Phys. Lett.* **35** 076802
[21] Guo Q, Wu Y, Xu L, Gong Y, Ou Y, Liu Y, Li L, Yan Y, Han G, Wang D, Wang L, Long S, Zhang B, Cao X, Yang S, Wang X, Huang Y, Liu T, Yu G, He K and Teng J 2020 *Chin. Phys. Lett.* **37** 057301
[22] Liu Q, Liu C X, Xu C, Qi X L and Zhang S C 2009 *Phys. Rev. Lett.* **102** 156603
[23] Zhu J J, Yao D X, Zhang S C and Chang K 2011 *Phys. Rev. Lett.* **106** 097201
[24] Tokura Y, Yasuda K and Tsukazaki A 2019 *Nat. Rev. Phys.* **1** 1
[25] Yu R, Zhang W, Zhang H J, Zhang S C, Dai X and Fang Z 2010 *Science* **329** 61
[26] Zhang D, Shi M, Zhu T, Xing D, Zhang H and Wang J 2019 *Phys. Rev. Lett.* **122** 206401
[27] Otrokov M M, Klimovskikh I I, Bentmann H, Estyunin D, Zeugner A, Aliev Z S, Gaß S, Wolter A U B, Koroleva A V, Shikin A M, Blanco-Rey M, Hoffmann M, Rusinov I P, Vyazovskaya A Y, Eremeev S V, Koroteev Y M, Kuznetsov V M, Freyse F, Sánchez-Barriga J, Amiraslanov I R, Babanly M B, Mamedov N T, Abdullayev N A, Zverev V N, Alfonsov A, Kataev V, Büchner B, Schwier E F, Kumar S, Kimura A, Petaccia L, Di Santo G, Vidal R C, Schatz S, Kißner K, Ünzelmann M, Min C H, Moser S, Peixoto T R F, Reinert F, Ernst A, Echenique P M, Isaeva A and Chulkov E V 2019 *Nature* **576** 416
[28] Gong Y, Guo J, Li J, Zhu K, Liao M, Liu X, Zhang Q, Gu L, Tang L, Feng X, Zhang D, Li W, Song C, Wang L, Yu P, Chen X, Wang Y, Yao H, Duan W, Xu Y, Zhang S C, Ma X, Xue Q K and He K 2019 *Chin. Phys. Lett.* **36** 076801
[29] Deng Y, Yu Y, Shi M Z, Guo Z, Xu Z, Wang J, Chen X H and Zhang Y 2020 *Science* **367** 895
[30] Li J, Li Y, Du S, Wang Z, Gu B L, Zhang S C, He K, Duan W and Xu Y 2019 *Sci. Adv.* **5** eaaw5685
[31] Zhang J, Wang D, Shi M, Zhu T, Zhang H and Wang J 2020 *Chin. Phys. Lett.* **37** 077304
[32] Pei C, Xia Y, Wu J, Zhao Y, Gao L, Ying T, Gao B, Li N, Yang W, Zhang D, Gou H, Chen Y, Hosono H, Li G and Qi Y 2020 *Chin. Phys. Lett.* **37** 066401
[33] Slater J C and Koster G F 1954 *Phys. Rev.* **94** 1498
[34] Zhang S H and Liu B G 2017 arXiv:1706.08943 [cond-mat.mes-hall]
[35] Kresse G and Joubert D 1999 *Phys. Rev. B* **59** 1758
[36] Perdew J P, Burke K and Ernzerhof M 1996 *Phys. Rev. Lett.* **77** 3865
[37] Sancho M P L, Sancho J M L and Rubio J 1985 *J. Phys. F* **15** 851
[38] Marzari N and Vanderbilt D 1997 *Phys. Rev. B* **56** 12847
[39] Mostofi A A, Yates J R, Lee Y S, Souza I, Vanderbilt D and Marzari N 2008 *Comput. Phys. Commun.* **178** 685
[40] Sun J, Zhong X, Cui W, Shi J, Hao J, Xu M and Li Y 2020 *Phys. Chem. Chem. Phys.* **22** 3128
[41] Cable J W, Wilkinson M K, Wollan E O and Koehler W C 1962 *Phys. Rev.* **127** 714
[42] Armbruster M, Ludwig T, Rotter H W, Thiele G and Oppermann H 2000 *Z. Anorg. Allg. Chem.* **626** 187
[43] Gregory N W 1951 *J. Am. Chem. Soc.* **73** 472
[44] Haastrup S, Strange M, Pandey M, Deilmann T, Schmidt P S, Hinsche N F, Gjerding M N, Torelli D, Larsen P M, Riis-Jensen A C, Gath J, Jacobsen K W, Mortensen J J, Olsen T and Thygesen K S 2018 *2D Mater.* **5** 042002
[45] McGuire M A 2017 *Crystals* **7** 121